Research Article

Sabri Alamri*, Paul A. Sürmann, Andrés F. Lasagni and Tim Kunze

Interference-based laser-induced micro-plasma ablation of glass

https://doi.org/10.1515/aot-2019-0061
Received November 18, 2019; accepted February 27, 2020; previously published online April 1, 2020

Abstract: Glass is one of the most important technical surfaces for numerous applications in automotive, optical, and consumer industries. In addition, by producing textured surfaces with periodic features in the micrometre range, new functions can be created. Although laser-based methods have shown to be capable to produce structured materials in a wide amount of materials, due to its transparency large bandgap dielectrics can be only processed in a controlled manner by employing high-power ultra-short pulsed lasers, thus limiting the employable laser sources. In this article, an interference-based method for the texturing of soda-lime glass using a 15 ns pulsed (1 kHz repetition rate) infrared (1053 nm) laser is proposed, which allows fabricating different periodic patterns with micrometre resolution. This method consists on irradiating a metallic absorber (stainless steel) put in direct contact with the glass sample and inducing locally an etching process on the backside of the glass. Then, the produced plasma at the interference maxima positions leads to the local fabrication of well-defined periodic line-like and dot-like surface patterns. The produced patterns are characterised using white light interferometry and scanning electron microscopy.

Keywords: direct laser interference patterning; glass; laser-induced microplasma; microstructuring.

***Corresponding author: Sabri Alamri,** Fraunhofer-Institut für Werkstoff- und Strahltechnik IWS, Winterbergstr. 28, 01277 Dresden, Germany, e-mail: sabri.alamri@iws.fraunhofer.de. https://orcid.org/0000-0003-3722-1942
Paul A. Sürmann and Tim Kunze: Fraunhofer-Institut für Werkstoff- und Strahltechnik IWS, Winterbergstr. 28, 01277 Dresden, Germany
Andrés F. Lasagni: Fraunhofer-Institut für Werkstoff- und Strahltechnik IWS, Winterbergstr. 28, 01277 Dresden, Germany; and Institut für Fertigungstechnik, Technische Universität Dresden, George-Bähr-Str. 3c, 01069 Dresden, Germany

www.degruyter.com/aot

1 Introduction

Glass materials are commonly used for their superior optical properties, surface stability and solvent compatibility. Furthermore, they can be easily processed, making them very attractive for a wide number of applications. In addition, functionalised glass surfaces with superhydrophobic/hydrophilic, anti-condensation or low-reflectance properties have increased their utilization in several fields including the automotive sector, electronics, and medical devices [1–3]. For example, due to its high resistance to mechanical stress, heat, and chemicals, microstructured fused silica and quartz find a common application in microfluidics, where micrometre-sized well-defined channels are necessary for guaranteeing the performances of the device [4, 5]. Moreover, fused silica is also one of the most suitable materials for the fabrication of optical elements containing microstructured areas as gratings, masks or filters [6]. Among transparent materials, also sapphire has been increasingly employed in several fields, ranging from optoelectronics to medicine, due to its high transparency, low residual stresses together with high chemical and physical resistance [7]. Microstructured sapphire finds its application in light-emitting devices [8], anti-reflective coatings for radiation in the far-IR range [9] and other structures for microelectronics, photonics, and microfluidics [10, 11]. In addition, it has been also demonstrated that using microstructured glass as substrate in thin-film Si solar cells permit increasing the scattering properties of the device, thus inducing a higher photon absorption and an overall higher efficiency [12].

Considerable efforts have been made for the development of simple, effective methods to fabricate micropatterns with resolution in the micron- or even nanometre-scale and with desirable surface properties. Among the most common methods for fabricating diffractive optical elements on fused silica is lithography, through which deep ultraviolet sources or electron beams are employed [13–15]. Through lithographic processes highly ordered and well defined microstructures can be fabricated, whose shape can be exactly controlled by processing parameters. Nevertheless, lithographic processes

involve multi-step fabrication steps and the use of chemicals for the etching phases [16].

Advanced surface functions are addressable for instance by surface texturing methods such as laser surface texturing. Compared with photolithographic and etching methods, laser micromachining presents a higher flexibility allowing a more efficient fabrication of tailored surface topographies [17].

Generally, the direct laser based processing of glasses require the use of either ultraviolet laser radiation with fluences higher than 10 J/cm^2 [18, 19] or laser sources providing ultra-short laser pulses, whose high peak intensities initiate nonlinear absorption processes [20, 21]. In the last case, also laser-induced periodic surface structures (LIPSS) have been observed on transparent materials like fused silica [22], soda-lime-silicate glass, and borosilicate glass by using fs-laser pulses [23], obtaining periodic patterns with spatial periods near to 1 μm. Although LIPSS can be relatively produced easily, the size of the periodic ripples remains in the range of the laser wavelength and microstructures with high depth are not easily achievable [24, 25].

An alternative to the above-mentioned methods is to treat the transparent substrates indirectly, utilizing an additional material (called absorber) which is capable to absorb the laser energy at the used laser wavelength, and is located in contact with the glass surface. Then, the laser radiation travels through the transparent material and induces etching on the backside of the target materials by means of the laser-generated plasma at the absorber's surface. This is the case of laser-induced backside wet etching (LIBWE), which has been already used to treat several transparent materials and in which liquid dyes are excited with UV-laser sources [26–29]. Particularly remarkable is the work of Zimmer et al. that employed liquid metals (as gallium or mercury) as absorbers, producing defined microstructures on fused silica [30, 31]. Although LIBWE has shown to have several advantages due to the absence of debris and cracks in the treated materials and the possibility to form metallic nanoparticles on the target material surface, this method necessitates the use of toxic liquids and high-power UV-lasers, which makes it less attractive for industrial applications [32–34]. Another possibility is to use laser-induced backside dry etching (LIBDE). In this case, the absorber material is a thin film (usually a metal) and similar excitation mechanisms can be induced, creating a plasma plume on the absorber's surface, capable to etch the backside of the target material. Due to the typical high absorption of metals used as absorbers, nanosecond infrared laser can be employed making LIBDE more favorable for industrial applications [35].

When the absorber is not in contact with the target material and the separation is comparable with the roughness of the surfaces, a confined plasma is created, which contains active species originated from the absorber and is localised in the region of space where the laser beam was focused [36, 37]. This method is described in the literature as laser-induced micro-plasma (LIMP) and microstructures can be fabricated on large bandgap dielectrics by the etching strength of the plasma expansion pressure. In fact, differently from free-expanding plasmas, confined plasmas present a higher expansion pressure [38] and the relation between etching rate and target distance, as well as a detailed description of the plasma's composition, have been investigated by Zhang and Veiko respectively [36, 39]. In case of higher separation between target material and absorber (up to several hundreds of micrometres), the technique takes the name of laser-induced plasma-assisted ablation (LIPAA), extensively investigated by Hanada et al., among others [40–44]. In this case, lower etching rate in the range of a few tens of nanometres per laser pulse are reached and metal deposition takes place on the backside of the target material simultaneously to the ablation [45]. Employing LIMP, several materials could be treated and structure depths up to 10 μm could be reached using alumina powder as absorber on solar glass, as demonstrated by Chao et al. [46]. Moreover, through the use of a phase-mask and a UV excimer laser, 1 μm periodic lines have been fabricated on quartz [47].

Considering the fabrication of periodic patterns with different length scales (larger or even smaller than the laser wavelength) other well-established laser-based texturing methods can be considered such as direct laser interference patterning (DLIP) [48, 49]. This method relies on the overlap of two or more coherent laser beams, whereby an interference pattern is created. For a given laser wavelength and number of beams, the spatial period can be easily adjusted by modifying the angle of the interfering beams, easily reaching in some optical configuration sub-micrometre periodic structures [50–53]. By changing the polarization and the geometrical configuration of the interfering beams, also very different pattern geometries can be created. In particular, in a two-beam arrangement a line-like pattern is generated, while employing four beams with the same polarization, angle and phase produces a dot-like intensity distribution with rectangular symmetry [50, 54]. In consequence, the combination of backside etching methods with the DLIP technology provides both the possibility to reach features smaller than the laser beam size and a better control of

their depth. This has been demonstrated for LIBWE in the works of Vass et al., where, employing deep UV nanosecond lasers, periodic lines where achieved on fused silica and transparent coatings, with a minimum periodicity of 104 nm and 1010 nm, respectively [55, 56]. In spite of the small size of the fabricated microstructures and high structuring homogeneity, a rectangular prism in immersion configuration is used in order to generate interference for very small periods, making the microstructuring approach less suitable for industrial purposes.

Here, a compact DLIP setup is used in LIMP configuration in order to texture soda-lime glass substrates, using stainless steel plates as absorber with an IR ns pulsed laser source. Line-like and dot-like periodic structures are fabricated using two and four beam optical configurations, and topographical surface analyses are systematically performed in order to elucidate the influence of the process parameters on the surface quality of the structures. The produced patterns are characterised using white light interferometry and scanning electron microscopy (SEM).

2 Materials and methods

For all the experiments, soda-lime glass slides (Carl Roth GmbH, Germany) with a transmissivity of 91.5% (between 400 and 1100 nm) and with an average roughness parameter Ra of 2.6 nm has been used. As the absorbing material, electro-polished austenitic 304 steel sheets (SG Designbleche GmbH, Germany) with an average roughness parameter Ra of 60 nm was utilised. As described in previous works, for increasing target-sample separation, the ablation rate decreases and the ablation threshold increases, lowering the efficiency of the texturing process [36, 41, 43, 44]. Therefore, the glass slides were put directly in contact with metal sheets without using any additional material. Moreover, in order to avoid relative motion between the glass slides and the metallic absorber, a special holder was constructed.

For the laser experiments, a compact diode-pumped Nd:YLF laser (Tech 1053 basic, Laser Export, Russia) emitting 15 ns pulses with TEM_{00} mode (Gaussian beam) at 1053 nm was used to irradiate the materials. Employing an IR laser source, a higher efficiency for the plasma generation and expansion was demonstrated. In fact, for the same pulse energy, a lower plasma ignition thresholds were reported for IR pulses in comparison with shorter wavelengths [57, 58]. The main laser beam was then directed through a compact DLIP optical module (Fraunhofer IWS, Germany), which produces irradiated areas containing the two or four-beam interference patterns (DLIP-pixels), generating line or dot-like patterns, respectively. The selection of the number of beams has been performed by masking two out of four beams inside the module. To cover larger areas than the DLIP-pixel (with a diametre of approximately ~90 μm), the sample was moved using high precision air-bearing linear motor stages (Aerotech PRO155-05, USA), with ±4 μm accuracy and ±0.4 μm repeatability. The structuring strategy involving the specific displacement of the DLIP-pixel has been already presented elsewhere [59]. For all experiments, a laser fluence of 3.3 J/cm² and a repetition rate of 1 kHz were employed. The laser fluence was calculated as the ratio between the employed average pulse energy (210 μJ) and the interference area at the working position (size of the DLIP-pixel). This last was determined through the D-squared method described by Liu [60].

After the fabrication process, the samples were rinsed with ethanol in ultrasonic bath for 30 min. The morphology of structured samples was characterised using white light interferometry (Leica DCM 3D) employing a 50x magnification objective, with lateral and vertical nominal resolution of 340 nm and 4 nm, respectively. Topographical measurements have been carried out using a Scanning Electron Microscope (SEM) at 5 kV of operation voltage (JEOL JSM 6610LV, Germany), after coating the samples with a 30 nm thick gold layer. The chemical composition of the laser-treated surfaces was analysed by energy dispersive X-ray spectroscopy (EDX).

3 Results and discussion

In the first set of experiments, soda-lime slides were placed over stainless steel sheets and irradiated with an interference pattern having a line-like or dot-like intensity distribution. In the case of line-like patterns, the DLIP-pixel was translated parallel to the interference pattern by an arbitrary pulse distance p and then moved laterally by a quantity h, called hatch distance. In particular, the hatch distance h must be set to a multiple integer of the spatial period Λ in order to guarantee a perfect period-to-period overlap (Figure 1A). The quantity p defines also the pulse-to-pulse overlap and can be expressed as number of pulses per pixel (P/px) which also denotes the cumulative fluence dose [61]. A similar procedure is applied for a dot-like pattern, with the difference that the pulse distance p is also equal to h, in order to perfectly match the previous dot-like pattern in both directions (Figure 1B). It is important to mention that, due to its rectangular symmetry, the periodic dots are arranged at 45° with respect to the orthogonal directions and for this reason the pulse distances are set as multiples of $\sqrt{2}\Lambda$. Moreover, the dot-like patterns were also re-irradiated multiple times (overscans) in order to increase the cumulative fluence dose.

A SEM image of the line-like texture produced on the glass substrate is shown in Figure 1C. In the experiment, the spatial period was set to 8.5 μm, using a pulse overlap of 26 pulses per pixel (P/px) and a hatch distance of one time the spatial period. As it can be noted, the produced microstructures on glass perfectly follow the imposed line-like intensity distribution, without significant variations of the structure depth, reaching high pattern homogeneity. Also in the case of four-beam interference (Figure 1D), the structuring parameters can be chosen in order to homogeneously cover areas larger than the DLIP-pixel itself, obtaining perfectly ordered 10.0 μm periodic dot-like structures.

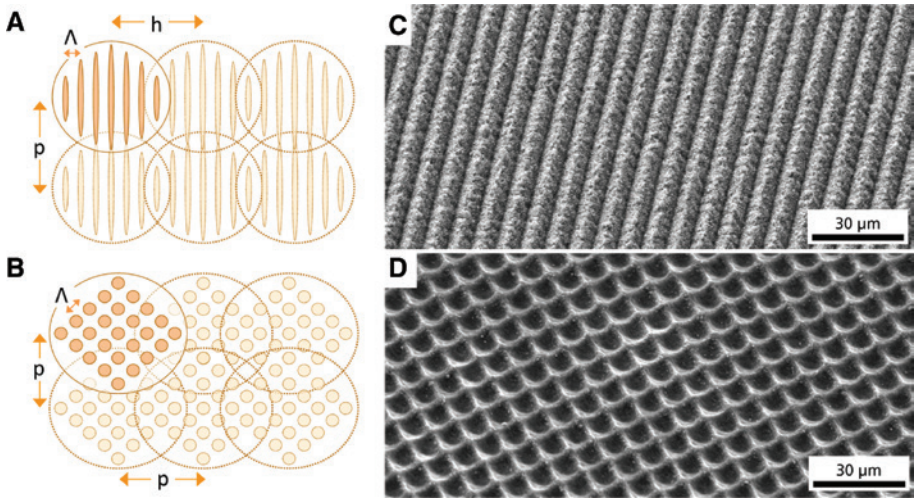

Figure 1: Pixel-wise structuring approach for a line-like (A) and dot-like (B) interference pattern. SEM images of (C) line-like (fluence: 3.3 J/cm², period: 8.5 µm, overlap: 26 P/px, hatch distance: 8.5 µm) and (D) dot-like (fluence: 3.3 J/cm², period: 10.0 µm, pulse distance: 10.0 µm, overscans: 10) patterns on soda-lime glass.

The mechanism involved in the structure formed at the glass substrate can be attributed to the LIMP process, confirming the hypothesis in this study. This implies that, due to the shape of the interference pattern, the ablation of the metallic absorber is induced only at the interference maxima positions the generated plasma locally etches the backside of the glass slide.

From Figure 1, it can also be noted that the spatial period imposed by the interference process and the one resulting on the glass surface perfectly matched. This is ascribable to the fact that the metal plate's roughness prevents a perfect glass-metal contact, thus leaving a thin air gap (Figure 2). In fact, assuming a perfect contact between glass and absorber, for the employed angle in two-beam interference (7.1°) a period of 12.75 µm would be expected, which considerably differs from the one found on the glass surface (8.5 µm). In consequence, the sub-beams are firstly refracted at the glass interface, thus changing their incident angle, and then due to the air-gap their recover their previous angle, meaning that the final interference angle is the same as the one of the incoming sub-beams at the glass surface.

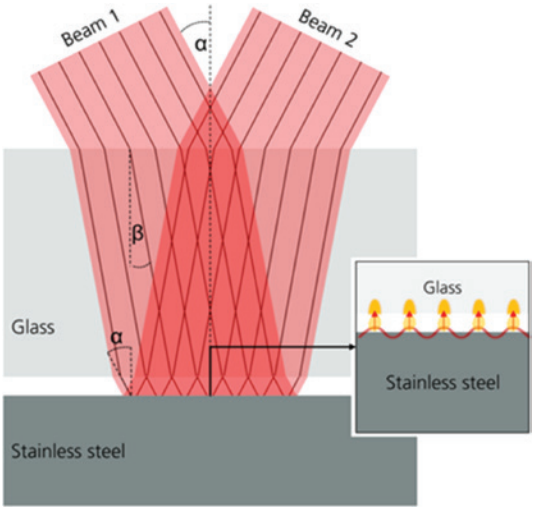

Figure 2: Scheme of the interference-based LIMP microstructuring mechanism using a glass sample and a stainless steel plate, between which the not perfect contact creates an air gap and allows recreating on the metal in the same interference angle as the one imposed on the glass surface.

In order to investigate the relationship between structure depth and texture quality in dependence on the structuring parameters, a systematic study was conducted, varying both the pulse and hatch distances. In particular, depending on the geometry the distances were set to a multiple of the spatial period as mentioned in the previous paragraph. This is relevant to avoid the creation of periodic inhomogeneities [59]. Figure 3A summarises the results of the line-like interference-based LIMP process with a spatial period of 8.5 µm in a contour diagram. This was obtained producing a 9×11 matrix, analysing the resulting structure depth (data-points marked in the diagram) and interpolating them through a 48 planes three-dimensional linear interpolation. It can be noticed that for low hatch distance and high overlap values, the structure depth reaches values of up to 4.4 µm which corresponds to an aspect ratio of ~0.5. In addition, the fabricated structures have been evaluated with respect to the overall structure quality, in particular whether a periodic modulation deriving from a specific hatch

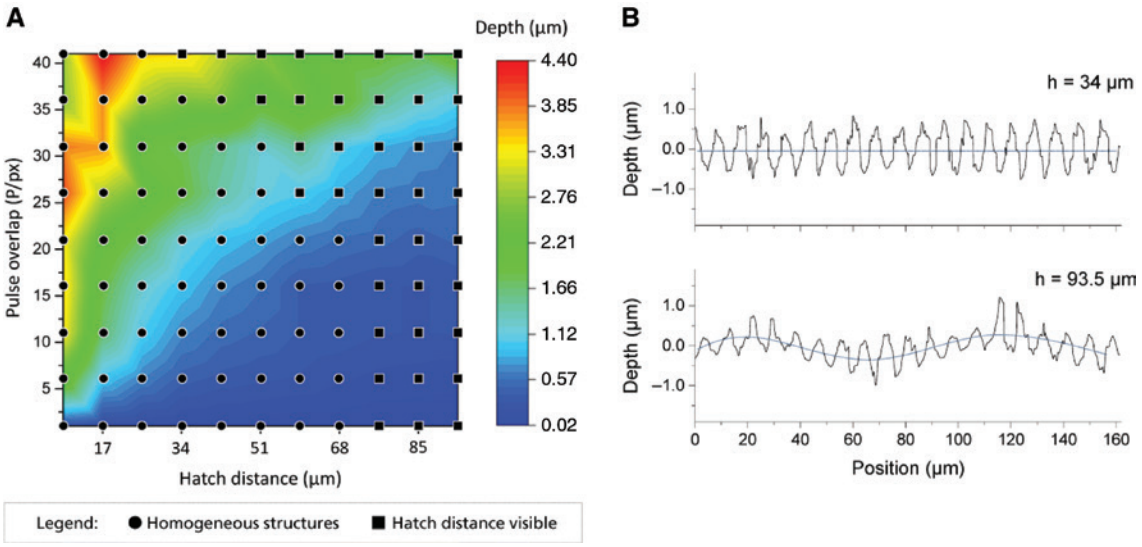

Figure 3: Structure depth as a function of the pulse overlap and hatch distance for the case of a line-like pattern with spatial period 8.5 µm (A) and examples of measured profiles of the fabricated structures with homogeneous and non-homogenous characteristics (B). The upper and lower profiles in (B) were produced with Fluence: 3.3 J/cm², period: 8.5 µm, overlap: 31 P/px, hatch distance: 34 µm and Fluence: 3.3 J/cm², period: 8.5 µm, overlap: 16 P/px, hatch distance: 93.5 µm, respectively (the lines are for guidance only).

distance is visible (squares in Figure 3A). For example, for hatch distance values higher than eight times the spatial period (68 µm), a periodic modulation comparable with the imposed hatch distance appears which reduces the overall homogeneity of the surface pattern. This can be ascribed to the laser beam profile (TEM_{00}) whose intensity decreases in the radial direction following a Gaussian distribution, which results in a modulation of the interference pattern itself, as described in a previous work [62]. Thus, microstructures with lower depth in the outer part of the DLIP-pixel are obtained, which influence the overall pattern homogeneity for large area texturing, as described by Aguilar-Morales et al. [59]. This effect can be better observed in Figure 3B, where a comparison between two texture profiles is reported. While the line-like structures fabricated with an high overlap corresponding to 31 P/px and a hatch distance of 34 µm (upper profile) any additional modulation is observed, the glass substrate treated with an low overlap of only 16 P/px and a hatch distance of 93.5 µm (lower profile) clearly shows also a low-frequency modulation, with a characteristic size which is comparable to the hatch distance used. Both types of morphologies are indicated with circles or squares in Figure 3A.

A similar study was conducted employing a four-beam interference-based LIMP processing scheme, creating an experimental 3×10 matrix and analysing it similarly to Figure 3A. The obtained results are summarised in Figure 4A for a spatial period of 10.0 µm. In particular, the pulse distance was varied up to three times the quantity $\sqrt{2}\Lambda$ (in both lateral directions) and the structured area was over-scanned multiple times (up to 10 times). The obtained results show that for low pulse distances and more than 5 overscans, the structure depth increases, reaching a maximum value of 2.8 µm. As for the line-like structuring, the choice of the pulse distance plays a fundamental role for the texture appearance, as reported in the two exemplar profiles in Figure 4B (overscans = 5). Also in this case, for low pulse distances (upper profile) textures with no additional modulation are created, while for pulse distances higher than 42.4 µm a modulation comparable with the pulse distance is visible.

In comparison with the line-like patterns produced with the two-beam interference-based LIMP configuration, an overall lower structure depth was reached. In order to better illustrate the differences between the line-like and dot-like textures, the variation of the mean structure depth has been represented as a function of the total amount of laser pulses in Figure 5. This was achieved using the structure depth data-points obtained in Figures 3A and 4A and taking into account the overlap among the laser pulses, distributed according to the schemes shown in Figure 1. The lower structure depth for dot-like structures can be ascribed to the lower amount of pulses used for a certain area (pulse per pixel), due to the necessity to keep the pulse overlap as a multiple integer of the spatial period in both directions for the four-beam configuration. For example, for line-like structures, a hatch distance of twice the spatial period and 41 pulses per pixels represents in total ~205 pulses

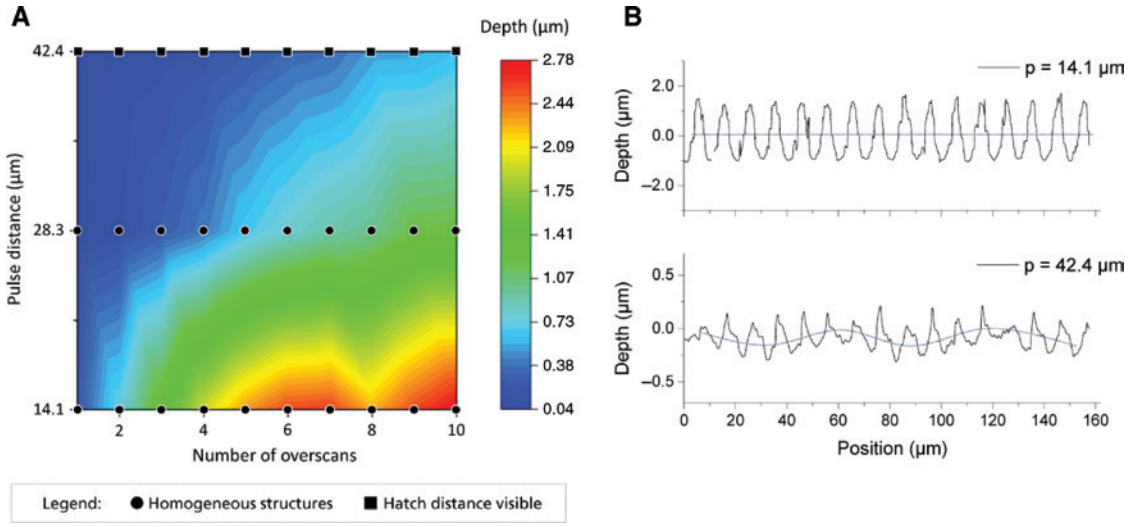

Figure 4: Structure depth as a function of the structuring parameters for the case of the dot-like pattern with spatial period 10.0 µm (A) and examples of measured profiles of the fabricated structures with homogeneous and non-homogenous characteristics (B). The upper and lower profiles in (B) were produced with fluence: 3.3 J/cm², period: 10.0 µm, pulse distance: 14.1 µm, overscans: 5 and fluence: 3.3 J/cm², period: 10.0 µm, pulse distance: 42.4 µm, overscans: 5, respectively (the lines are for guidance only).

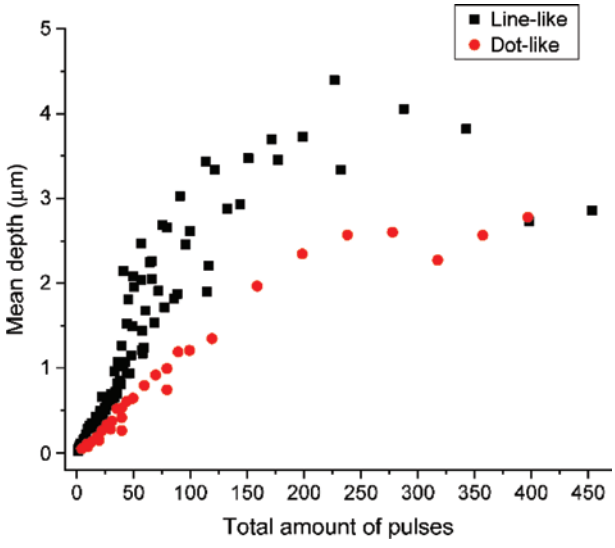

Figure 5: Evolution of the mean structure depth as a function of the total amount of laser pulses for 8.5 µm line-like and 10.0 µm dot-like textures fabricated on soda-lime glass.

impinging the same position, leading to structure depths of 4.4 µm. In the case of dot-like pattern, a single scan with a pulse distance of one time the spatial period translates to only ~40 pulses per pixel, which yields a structure depth lower than 0.3 µm. Furthermore, although by increasing the number of overscans the structure depth increases accordingly, the evolution is not linear and the deepest produced hole-like patterns were 2.8 µm in depth. In particular, this depth was obtained with 10 overscans and a pulse distance of one time the quantity $\sqrt{2}\Lambda$, representing theoretically ~400 total pulses. The low effectiveness of the overscans could be ascribed to the presence of the pre-textured surface when successive overscans follow the first structuring step, which might result in diffraction of the laser radiation and thus a reduction of the effective fluence dose.

As for the line-like structuring, the aspect ratio of the dot-like structures sensibly depends on the employed pulse distance, producing a structure depth of 0.4 µm and 2.8 µm when using a pulse distance of three and one time the quantity $\sqrt{2}\Lambda$, respectively. This observation can be traced back to the different total amount of laser pulses per area (i.e. the total fluence dose) with which the structuring is carried out. In particular for a single scan, a pulse distance of three times the period corresponds to 7 P/px and a pulse distance of one time the period to 63 P/px, thus creating a much rougher texture in the second case than in the first due to the higher fluence dose.

In addition to the depth of the structures, the amount of used laser pulses also influences the morphology of the produced periodic arrays. A comparison between the fabricated line-like microstructures at two different processing conditions is shown in Figure 6A and B for a period of 8.5 µm and a hatch distance of twice the spatial period. For low pulse overlap (6 P/px, Figure 6A) the structure appears shallow and barely visible, while employing a higher overlap (41 P/px, Figure 6B) results in deeper microstructures with an additional roughness, especially at the interference minima positions (i.e. at the areas surrounding the ablated lines). A similar behaviour can be noticed

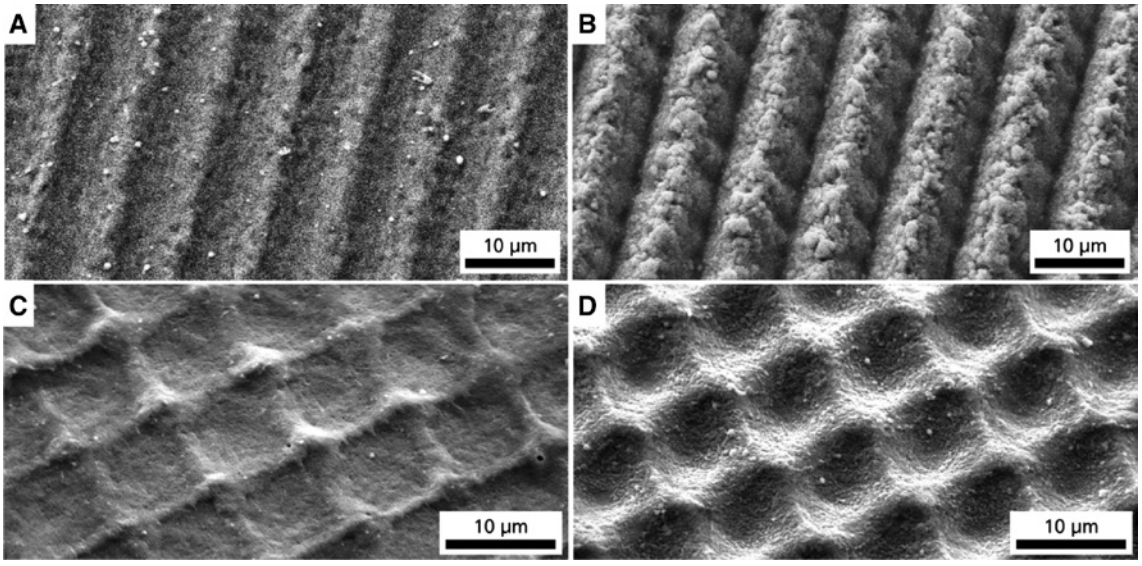

Figure 6: Secondary electron micrographs showing the comparison between 8.5 µm line-like textures on soda-lime glass for low (6 P/px) (A) and high (41 P/px) (B) overlap conditions, and dot-like textures fabricated using a pulse distance of 42.4 µm (C) and 14.1 µm (D) and 10 overscans. The used laser fluence per pulse was 3.3 J/cm^2.

for the dot-like microstructures, comparing the textures fabricated with pulse distances of 42.4 µm (Figure 6C) and 14.1 µm (Figure 6D), applying 10 overscans in both cases. The increase of the surface roughness for high pulse overlap values can be also attributed to the higher quantity of reactive species formed in the etching plasma.

Moreover, deposited material in the form of particle clusters is also visible in the presented SEM images, which are possibly metallic particles coming from the etched absorber's surface. In order to prove the assumption and assess the cleanliness of treated regions, EDX measurement have been carried out on the glass surface patterned with 8.5 µm line-like structures employing an overlap of 21 P/px and a hatch distance also of 8.5 µm. To enhance the contrast between glass and any external contaminant, backscattered electrons images have been acquired (Figure 7A) where bright spots can be identified, which on first examination can be ascribed to metal particles. In the same area, the signals of silicon (Kα1), iron (Lα1,2) and oxygen (Kα1) have been mapped (Figure 7B, C and D, respectively). As it can be observed, the oxygen signal (Figure 7D) is homogenously distributed all over the analysed area except in the regions where particles are located. Differently, the intensity for Si (Figure 7B) decreases at the positions corresponding to the topography heights (interference minima) as well as in the regions where the particles are located. Regarding the Fe intensity map, the opposite behaviour was observed (Figure 7C). In consequence, it can be deducted that the particles observed in the image correspond to Fe (unoxidised) transferred from the metallic substrate to the glass material. These large particle clusters are typically caused due to the physical ejection of part of the absorber material due to the creation of shock waves during the ablation process [34].

Regarding the increase of the intensity of Fe at the topography heights (which is complementary to the Si signal) as well as considering that the intensity of oxygen is not affected at these positions, we suggest that the observed chemical signals correspond to iron in oxidised form. In fact, the deposition of oxidised metal particles can be explained considering the origination and expansion of the plasma generated by the sine-like laser intensity distribution. In this context, the plasma, rich in metallic species originated by the stainless steel [63], expands following the imposed line-like pattern, directly etching the glass in the central region of the micro-lines (interference maxima) and depositing oxidised metal particles where the intensity is lower (interference minima). The oxidation can be explained taking into account the relative long pulses (15 ns) employed, which is typical phenomenon for the laser ablation of metals in the nanosecond regime [64, 65].

4 Conclusions

Line-like and dot-like periodic micro-structures were fabricated on a soda-lime glass using DLIP combined with the

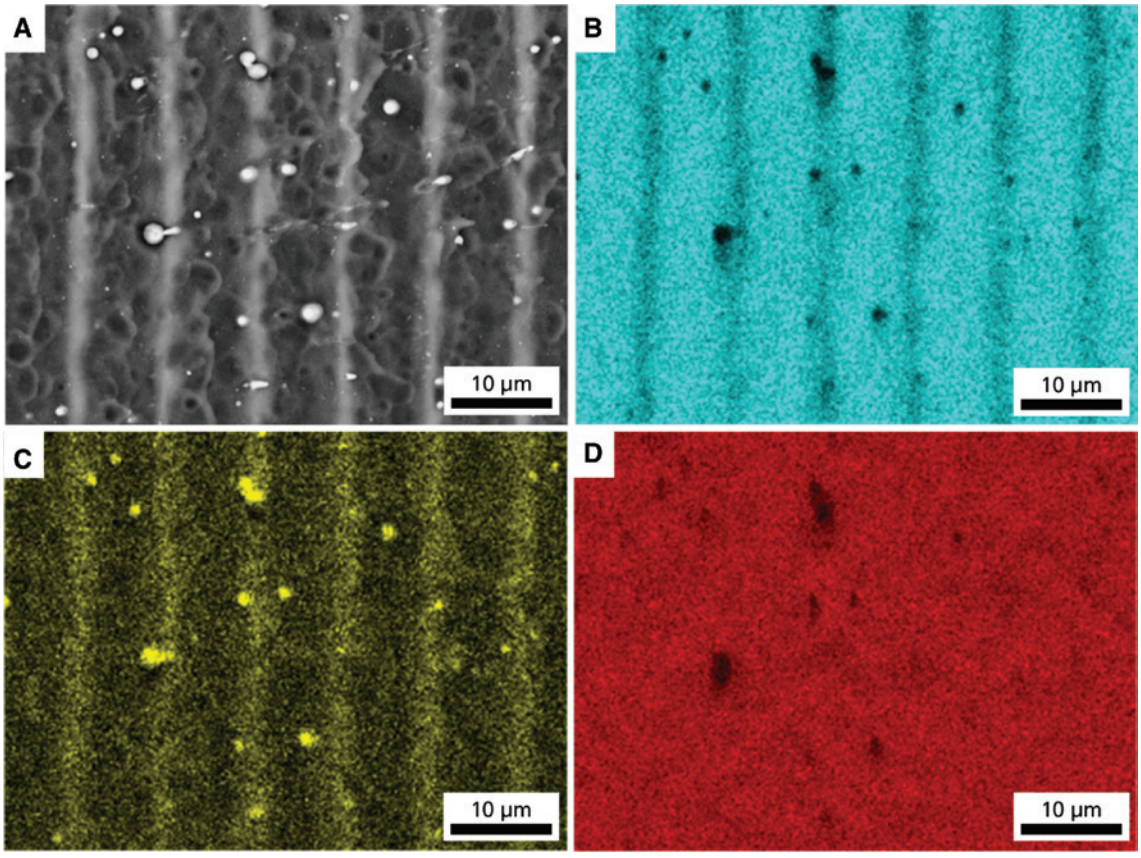

Figure 7: Backscatter SEM image of a glass surface textured through the interference-based LIMP (A) and the respective EDX-mapping for the signals Si-Kα1 (B), Fe-Lα1,2 (C) and O-Kα1 (D). The employed structuring parameters were: spatial period = 8.5 µm; overlap = 21 P/px; hatch distance = 8.5 µm.

LIMP structuring approach. The glass slides were placed on a flat metal absorber of stainless steel and irradiated with different periodic energy distributions, generated by a nanosecond pulsed infrared laser. In both cases, it was observed that the glass material was locally etched on the backside locally at the interference maxima positions, creating microstructures that perfectly follow the incoming interference intensity distribution. A systematic variation of the structuring parameters, together with the topographical analyses, permitted to assess the surface quality of the produced structures and to identify the factors for which the textures appear homogeneous and well-defined. For example, surfaces textured with high hatch distances presented a low-frequency modulation with a period of the same value. When using structuring parameters such high pulse overlaps, deeper surface textures were obtained, however, in most of the cases they were covered with an additional roughness (in the nanometre range), which is ascribable to a more intense etching process characterised by redeposition of metallic particles in the glass' surface. Further studies will be carried out, involving the use of different absorber materials, as well as a detailed chemical analysis of the glass surfaces resulting after this indirect interference-based process.

Acknowledgments: The work of A. F. L. is supported by the German Research Foundation (DFG) under Excellence Initiative program by the German federal and state governments to promote top-level research at German universities. The authors acknowledge J. Bretschneider (Fraunhofer IWS) for the EDX analyses.

Author contributions: All the authors contributed equally to the scientific discussions and revision of the manuscript. S. A. designed the experiments, acquired SEM images and wrote the manuscript. P. A. S. performed the main structuring experiments and the data analysis. A. F. L. and T. K. directed the research activities.

References

[1] H. K. Raut, V. A. Ganesh, A. S. Nair and S. Ramakrishna, Energy Environ. Sci. 4, 3779 (2011).

[2] S. Chattopadhyay, Y. F. Huang, Y. J. Jen, A. Ganguly, K. H. Chen, et al., Mater. Sci. Eng. R Reports 69, 1 (2010).
[3] X. Zhang, F. Shi, J. Niu, Y. Jiang and Z. Wang, J. Mater. Chem. 18, 621 (2008).
[4] A. Grosse, M. Grewe and H. Fouckhardt, J. Micromech. Microeng. 11, 257 (2001).
[5] T. Ujiie, T. Kikuchi, T. Ichiki and Y. Horiike, Japanese J. Appl. Physics, Part 1 Regul. Pap. Short Notes Rev. Pap. 39, 3677 (2000).
[6] N. P. Bansal and R. H. Doremus, Handbook of Glass Properties (Academic Press, Inc., Orlando, Florida, 1986).
[7] Z. C. Li, Z. J. Pei and P. D. Funkenbusch, in Proc. Inst. Mech. Eng. Part B J. Eng. Manuf. 255, (2011) pp. 975–989.
[8] L. Kuna, A. Haase, F. Reil, C. Sommer, J. R. Krenn, et al., IEEE J. Sel. Top. Quantum Electron. 15, 1250 (2009).
[9] T. Matsumura, K. Young, Q. Wen, S. Hanany, H. Ishino, et al., Appl. Opt. 55, 3502 (2016).
[10] D. Wortmann, J. Gottmann, N. Brandt and H. Horn-Solle, in 2008 Conf. Quantum Electron. Laser Sci. Conf. Lasers Electro-Optics, CLEO/QELS (2008).
[11] S. Juodkazis, SPIE Newsroom 510 (2007). Available at: https://www.researchgate.net/profile/Saulius_Juodkazis/publication/249515811_Forming_tiny_3D_structures_for_micro-_and_nanofluidics/links/5597f7f308ae99aa62ca1b36.pdf.
[12] S. Venkataraj, J. Wang, P. Vayalakkara and A. G. Aberle, IEEE J. Photovoltaics 3, 605 (2013).
[13] S. Franssila, Introduction to Microfabrication (John Wiley & Sons, Ltd., Chichester, UK, 2010).
[14] M. Rothschild, in Conf. Lasers Electro-Optics Eur. - Tech. Dig. 6 (IEEE Cat. No. 98CH36178), 122 (1998).
[15] T. Clausnitzer, J. Limpert, K. Zöllner, H. Zellmer, H.-J. Fuchs, et al., Appl. Opt. 42, 6934 (2003).
[16] T. Ito and S. Okazaki, Nature 406, 1027 (2000).
[17] D. Bäuerle, Laser Processing and Chemistry (Springer Science & Business Media, Heidelberg, 2013).
[18] J. Ihlemann, B. Wolff and P. Simon, Appl. Phys. A Solids Surfaces 54, 363 (1992).
[19] J. Ihlemann and B. Wolff-Rottke, Appl. Surf. Sci. 106, 282 (1996).
[20] D. Du, X. Liu, G. Korn, J. Squier and G. Mourou, Appl. Phys. Lett. 64, 3071 (1994).
[21] R. Stoian, M. Boyle, A. Thoss, A. Rosenfeld, G. Korn, et al., Appl. Phys. Lett. 80, 353 (2002).
[22] A. Rosenfeld, M. Rohloff, S. Höhm, J. Krüger and J. Bonse, Appl. Surf. Sci. 258, 9233–9236 (2012).
[23] S. Gräf, C. Kunz and F. A. Müller, Materials 9, 476 (2016).
[24] J. Bonse, S. V. Kirner, S. Höhm, N. Epperlein, D. Spaltmann, et al., Laser-based Micro- Nanoprocessing XI 10092, 100920N (2017).
[25] I. Gnilitskyi, T. J. Y. Derrien, Y. Levy, N. M. Bulgakova, T. Mocek, et al., Sci. Rep. 7, 1 (2017).
[26] H. Niino, Y. Yasui, X. Ding, A. Narazaki, T. Sato, et al., J. Photochem. Photobiol. A Chem. 158, 179 (2003).
[27] T. Sato, R. Kurosaki, Y. Kawaguchi, A. Narazaki and H. Niino, J. Laser Micro Nanoeng. 5, 256 (2010).
[28] H. Niino, Y. Kawaguchi, T. Sato, A. Narazaki, T. Gumpenberger, et al., J. Phys. Conf. Ser. 59, 539 (2007).
[29] K. Zimmer, R. Böhme and B. Rauschenbach, Appl. Phys. A 79, 1883 (2004).
[30] K. Zimmer, R. Böhme, D. Ruthe and B. Rauschenbach, Appl. Phys. A 84, 455 (2006).
[31] K. Zimmer, R. Böhme, D. Hirsch and B. Rauschenbach, J. Phys. D. Appl. Phys. 39, 4651 (2006).
[32] J. Wang, H. Niino and A. Yabe, Appl. Phys. A Mater. Sci. Process. 69, S271–S273 (1999).
[33] O. M. Zhigalina, D. N. Khmelenin, A. V. Atanova, N. V. Minaev, A. P. Sviridov, et al., Plasmonics 1, 1–10 (2019).
[34] M. Y. Tsvetkov, V. I. Yusupov, P. S. Timashev, K. M. Golant, N. V. Minaev, et al., Nanotechnol. Russ. 12, 86 (2017).
[35] P. Lorenz, M. Ehrhardt and K. Zimmer, Appl. Surf. Sci. 258, 9742 (2012).
[36] J. Zhang, K. Sugioka and K. Midorikawa, Appl. Phys. A Mater. Sci. Process. 67, 545 (1998).
[37] V. A. Shkuratova, G. K. Kostyuk, M. M. Sergeev, R. A. Zakoldaev and E. B. Yakovlev, Opt. Mater. Express 9, 2392 (2019).
[38] R. Fabbro, J. Fournier, P. Ballard, D. Devaux and J. Virmont, J. Appl. Phys. 68, 775 (1990).
[39] V. P. Veiko, S. A. Volkov, R. A. Zakoldaev, M. M. Sergeev, A. A. Samokhvalov, et al., Quantum Electron. 47, 842 (2017).
[40] Y. Hanada, K. Sugioka and K. Midorikawa, in High-Power Laser Ablation VI, 6261 (2006) p. 626111.
[41] Y. Hanada, K. Sugioka, Y. Gomi, H. Yamaoka, O. Otsuki, et al., Appl. Phys. A Mater. Sci. Process 79, 1001–1003 (2004).
[42] T. Smausz, T. Csizmadia, N. Kresz, C. Vass, Z. Márton, et al., Appl. Surf. Sci. 254, 1091 (2007).
[43] A. H. Hamdani, W. Ahmed, A. Ansar, R. Akhter, W. A. Farooq, et al., Key Eng. Mater. 442, 172 (2010).
[44] A. H. Hamdani, A. Nasir, S. Sarwar, A. Ansar, R. Akhter, et al., J. Phys. Conf. Ser. 439, 1 (2013).
[45] Y. Hanada, K. Sugioka, H. Takase, H. Takai, I. Miyamoto, et al., Appl. Phys. A Mater. Sci. Process. 80, 111 (2005).
[46] H. Chao, L. Furong, W. Min, Y. Jianwen and C. Jimin, J. Laser Appl. 24, 022005 (2012).
[47] J. Zhang, K. Sugioka and K. Midorikawa, Opt. Lett. 23, 1486 (1998).
[48] Y. Nakata, Adv. Opt. Techn. 2, 2–6 (2016).
[49] B. Voisiat, M. Gedvilas, S. Indrišiunas and G. Raciukaitis, J. Laser Micro Nanoeng. 6, 185 (2011).
[50] B. Voisiat, M. Gedvilas, S. Indrišinas and G. Račiukaitis, Phys. Procedia 12, 116 (2011).
[51] J. Bekesi, J. Meinertz, J. Ihlemann and P. Simon, Appl. Phys. A Mater. Sci. Process. 93, 27 (2008).
[52] J. H. Klein-Wiele and P. Simon, Appl. Phys. Lett. 83, 4707 (2003).
[53] J. Bekesi, P. Simon and J. Ihlemann, Appl. Phys. A Mater. Sci. Process. 114, 69 (2014).
[54] A. Fernandez and D. W. Phillion, Appl. Opt. 37, 473 (1998).
[55] C. Vass, K. Osvay, T. Véso, B. Hopp and Z. Bor, Appl. Phys. A Mater. Sci. Process. 93, 69 (2008).
[56] B. Kiss, F. Ujhelyi, Á. Sipos, B. Farkas, P. Dombi, et al., J. Laser Micro Nanoeng. 8, 271 (2013).
[57] L. M. Cabalin and J. J. Laserna, Spectrochim. acta, Part B At. Spectrosc. 53, 723 (1998).
[58] A. E. Hussein, P. K. Diwakar, S. S. Harilal and A. Hassanein, J. Appl. Phys. 113, 143305 (2013).
[59] A. I. Aguilar-morales, S. Alamri, T. Kunze and A. F. Lasagni, Opt. Laser Technol. 107, 216 (2018).
[60] J. M. Liu, Opt. Lett. 7, 196 (1982).
[61] S. Alamri, A. I. Aguilar-Morales and A. F. Lasagni, Eur. Polym. J. 99, 27 (2018).
[62] S. Alamri and A. F. Lasagni, Opt. Express 25, 9603 (2017).
[63] S. Palanco, J. J. Laserna and J. M. Baena, Spectrochim. Acta – Part B At. Spectrosc. 57, 591 (2002).

[64] V. Veiko, Y. Karlagina, M. Moskvin, V. Mikhailovskii, G. Odintsova, et al., Opt. Lasers Eng. 96, 63 (2017).
[65] D. P. Adams, V. C. Hodges, D. A. Hirschfeld, M. A. Rodriguez, J. P. McDonald, et al., Surf. Coatings Technol. 222, 1 (2013).

Sabri Alamri
Fraunhofer-Institut für Werkstoff- und Strahltechnik IWS, Winterbergstr. 28, 01277 Dresden, Germany
sabri.alamri@iws.fraunhofer.de
https://orcid.org/0000-0003-3722-1942

Sabri Alamri is a doctoral researcher in the group of Surface Functionalization at the Fraunhofer IWS (Germany), and at the Institute for Manufacturing Technology of the Technical University of Dresden since 03/2016. His main expertise is in the field of laser surface structuring, in particular Direct Laser Interference Patterning, optical design and analytical methods. Currently his research interests are focused in the fabrication of functional surfaces employing polymeric and non-metallic materials, as well as in the modelling of laser-matter interaction processes.

Paul A. Sürmann
Fraunhofer-Institut für Werkstoff- und Strahltechnik IWS, Winterbergstr. 28, 01277 Dresden, Germany

Paul A. Sürmann is a student of production engineering at the Mechanical Engineering faculty of the Technical University of Dresden since 10/2013 and is a student researcher at the Fraunhofer IWS (Germany) since 2019. His research topic focusses on the field of laser micro texturing of transparent materials surfaces with Direct Laser Interference Patterning employing direct and indirect structuring approaches.

Andrés F. Lasagni
Fraunhofer-Institut für Werkstoff- und Strahltechnik IWS, Winterbergstr. 28, 01277 Dresden, Germany; and Institut für Fertigungstechnik, Technische Universität Dresden, George-Bähr-Str. 3c, 01069 Dresden, Germany

Andrés F. Lasagni received in 2002 his MS degree in Chemical Engineering from the Comahue National University (Argentina). From 2003 to 2005 he carried out his PhD at Saarland University (Germany) and in 2007–2008 he conducted a postdoctoral stay at the Georgia Institute of Technology and the University of Michigan. Since 2012 he is professor at the Technische Unversität Dresden (Germany). A. F. L. is author/coauthor of more than 250 publications and has been awarded with several prizes including the German High Tech Champion in Photovoltaic 2011, the Green Photonic Award and the FEMS Innovation award 2017.

Tim Kunze
Fraunhofer-Institut für Werkstoff- und Strahltechnik IWS, Winterbergstr. 28, 01277 Dresden, Germany

Tim Kunze received his MS degree in Computational Science from the TU in Chemnitz (Germany) in 2008. From 2009 to 2013 he carried out his PhD at TU Dresden (Germany) focusing on tribology simulation. In 2014, he joined the Fraunhofer Institute of Material and Beam Technology (IWS) in Dresden as a senior researcher involved in the R&D of Direct Laser Interference Patterning technology. In 2016, his contribution within the project group DLIP was awarded with the 2nd place of the 'Berthold Leibinger Innovationspreis 2016' (Germany). Since September 2017, Dr. Kunze leads the group surface functionalization at Fraunhofer IWS Dresden.